DOI: https://doi.org/10.5592/CO/EUROENGEO.2024.288

# DEFORMATION FORECASTING AND STABILITY ANALYSIS OF SOFT ROCK TUNNEL FORM MICROSESMIC SOURCE PROBABILISTIC LOCALIZATION

YUEPENG SUN [1], NUWEN XU [2], BIAO LI [3], PEIWEI XIAO [4], ZHIQIANG SUN[5]…

[1] *Sichuan university, China, People's Republic of, ypsun1997@163.com*

[2] *Sichuan university, China, People's Republic of, xunuwen@scu.edu.cn*

[3] *Southwest Petroleum University, China, People's Republic of, libiaoscu@163.com*

[4] *Sichuan university, China, People's Republic of, xpwsl@163.com*

[5] *Sinohydro Bureau 7 Co., Ltd., China, People's Republic of, 345178218@qq.com*

**Abstract**

Surrounding rock deterioration and large deformation have always been a significant difficulty in designing and constructing tunnels in soft rock. The key lies in real-time perception and quantitative assessment of the damaged area around the tunnel. An in-situ microseismic (MS) monitoring system is established in the plateau soft tock tunnel. In this paper, the probability density field of MS source based on probability mapping is proposed, which lays a foundation for accurately revealing the progressive damage characteristics of soft rock tunnel. The spatial distribution of MS dissipative energy is established. The morphological evolution of tunnel with multiple damage degrees in axial and radial direction is analyzed. Based on the basics MS energy parameter,a three-dimensional model was created to visualize the damage zone of the tunnel surrounding rock. The model depicted varying degrees of damage, and three high damage zones were identified. The rapid increase of the depth and extent of high damage area can be used as the criterion of dynamic warning of large deformation of surrounding rock of tunnel. This paper provides valuable insights for damage and dynamic warning of surrounding rock of high-stress soft rock tunnel.

**Key words**

Soft rock tunnel, MS monitoring, Seismic source location, Excavation damage zone.

## 1 Introduction

With the growth of the global economy and the increasing demand for modernization, tunnels have emerged as a highly favorable option for constructing transportation infrastructure in intricate topographical conditions (Yu et al., 2022). China's road transport network has extended tunnels to high mountainous areas in recent years, resulting in long lines (length exceeding 10 km) and deep burial (depth exceeding 500 m), making it impossible to avoid complex geological features and poor ground layers (Du et al., 2023; Zhu et al., 2019). When a tunnel passes through soft rock, such as carbonaceous slate, mudstone, etc., with high in-situ stress, the surrounding rock mass experiences time-dependent extrusion deformation and fracturing due to intense internal extrusion and excavation loading; this phenomenon of the surrounding rock in the tunnel is characterized by long-term non-convergence of deformations, leading to issues such as spray concrete cracking, arch distortion, and deformation invading limit (Figure 1). These problems significantly impede the safety and efficiency of tunnel construction, resulting in substantial economic losses and delays in project completion (Kang et al., 2022; Yu et al., 2023; He et al., 2022). For soft rock tunnels, investigating the progressive deformation and failure mechanism in soft rockmass around the tunnel is crucial for predicting, evaluating, and ensuring the safety of soft rock tunnels subjected to high-ground stress.

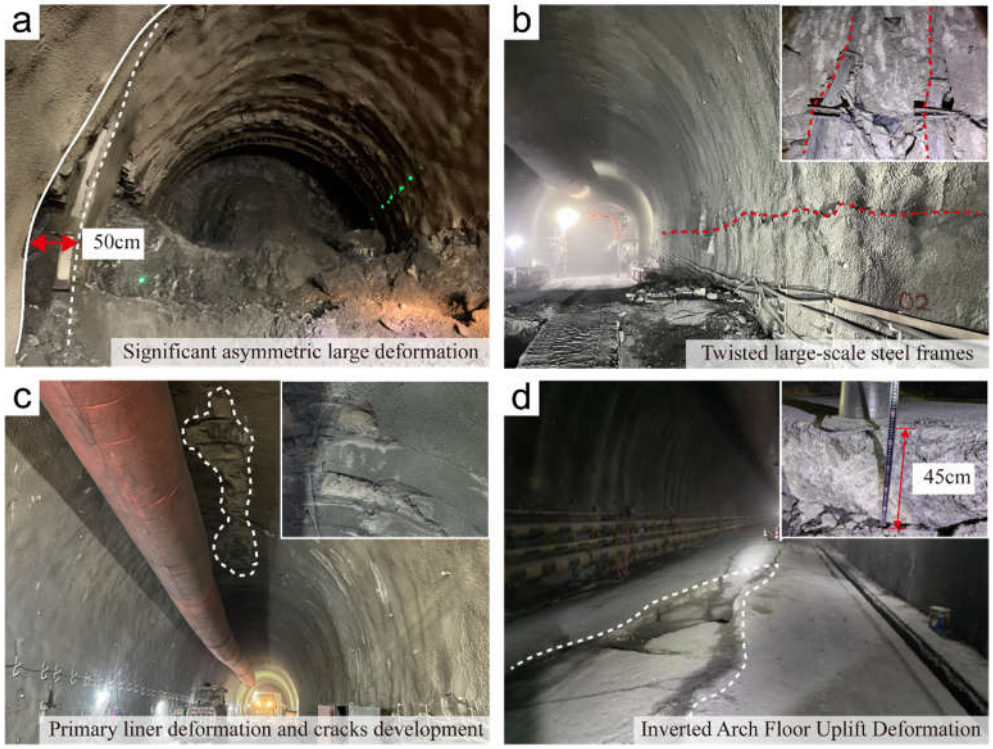


**Figure 1.** Large deformation and typical failure characteristics of supporting structure of tunnel project.

The railway tunnel studied in this research is located on the edge of the Qinghai-Tibet Plateau and the Sichuan Basin, one of the world's most active areas of neotectonic movement (Wang and Barbot, 2023). Tectonically, due to the collision between the Indian Ocean plate and the Eurasian plate, the geological tectonic activity in the tunnel's location is intense, the geological conditions are complex, and the in-situ stress is high. (Chen et al., 2023). The area studied in this research is the No.4 auxiliary tunnel. Figure 1a shows the longitudinal profile of the No.4 auxiliary tunnel by approximately 1600 m. The exit chainage (vertical projection distance of the route) is 0+000 m, and the entrance chainage is 1+642 m, and the longitudinal slope is 0.67%. The cross-sections of the No.4 auxiliary tunnel are both in the shape of a city gate. A combination of the micro bench cut method and traditional drilling and blasting excavates the auxiliary tunnels. The lithology of the strata traversed by the tunnel is mainly carbonaceous phyllite, sandstone, with thin layered structure distribution and distorted rock formation. Due to internal and external geological dynamic disturbance and the influence of excavation unloading, the stability of fractured carbonaceous phyllite is weak. The average uniaxial compressive strength of the carbonaceous slate obtained from the field point load testing ranges from 1.60 to 10.83 MPa (Hathway, 2009). The uniaxial compressive strength measured in different regions varies greatly, and the standard deviation of data is 2.739 MPa. The stability of tunnel's surrounding rock is adversely affected by a combination of intricate geological conditions, the presence of thin layers of surrounding rock, elevated ground stress, and the presence of soft rock mass.

A comprehensive understanding of the internal structure of the surrounding rock mass and its dynamic evolution, including fracture field, displacement field, and stress field, is challenging due to the complexity and invisibility of the interior. MS monitoring technology, a three-dimensional and non-destructive monitoring method, can monitor real-time micro-fracture initiation, development, expansion, and failure in the rock mass. This technology also helps in understanding the weakening of mechanical properties caused by the accumulation of rock damage (Mngadi et al., 2019). Feng et al. (2022) recognized deep engineering rock mass's internal aging deformation and failure process through in-situ MS monitoring. Chen et al. (2018) identified the time, intensity and extent of initial crack and breakage in soft rock tunnel by analyzing the frequency and energy evolution of MS events. Regrettably,

the authors have not adequately elucidated soft rock tunnels' fracturing expansion and squeezing deformation. Consequently, current research aims to employ MS monitoring to comprehensively investigate the precise geographic extent and configuration of failure in soft rock tunnels. Additionally, authors seek to forecast and monitor significant deformations within soft rock tunnels.

This paper presents a practical application of MS monitoring in the safety management of large deformations caused by fracturing and squeezing the surrounding rock in a soft rock tunnel in Southwest China. A real-time MS monitoring system was utilized to analyze the initiation, propagation, and the disparities and expansion characteristics of fractured and damaged zones during various construction periods. This study integrates DEM simulation method with quantification of MS source mechanisms to elucidate the mechanism behind significant deformation disasters resulting from fracture development in surrounding rocks during intense unloading conditions. The findings provide an important case study that can contribute to predicting massive deformation accurately as well as implementing precise support measures in soft rock tunnels.

## 2 Methods

### 2.1 MS monitoring scheme and performance test

The MS monitoring system manufactured by the Engineering Seismology Group (ESG), Canada, was installed on December 7, 2022 and has been in operation since then. The MS monitoring network is composed of six single-axis accelerometers with natural frequency of 10khz, Paladin digital signal acquisition system and Hyperion digital signal processing system. All accelerometer cables are connected to a Paladin digital signal acquisition system. The Paladin data acquisition component gathers data in real-time and sends it to the Hyperion digital signal processing system via a communication cable. Figure 2 shows a multi–channel MS monitoring in plateau soft tock tunnel following the suggested approach by the in-situ investigations and the ISRM suggested method (Feng et al., 2019). Due to space, staffing, and safety equipment constraints, the MS sensor was distributed on the two junctions behind the working face, 30m apart. The first row of sensors was 30 meters from the tunnel's working face. When the working face moved 30 m forward, the row of sensors farthest from the work area were recycled and then put in a place 30 m away from later working face.

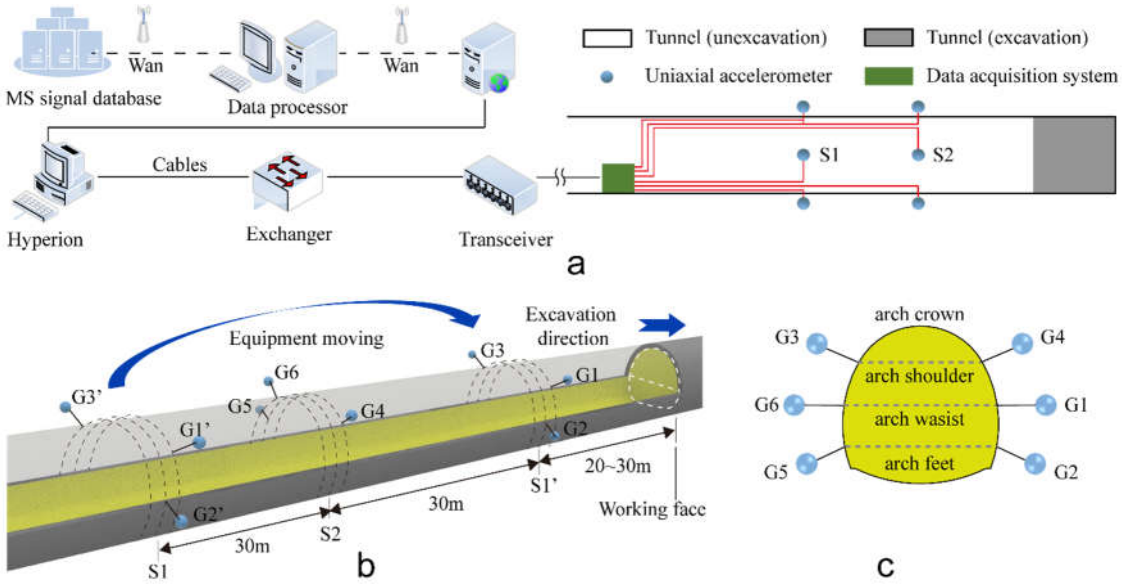


**Figure 2.** The MS monitoring system configuration. (a) Topology of MS monitoring network. (b) Moving diagram of field accelerometer sensor. (c) Front view of the layout of accelerometer sensors.

Figure 3 illustrates the signals the MS monitoring system acquired within the monitored area.

Identification of the effective MS signal requires detailed waveform analysis in both the time and frequency domains. Fig. 4a illustrates working face excavation blasting on March 4, 2023. The signal lasted 0.4 seconds and had a maximum amplitude of 4 volts. In the time-frequency domain, MS events have a significant frequency distribution from 100 to 1500 Hz, with a concentration from 200 to 900 Hz. The dominant frequency is 476.667 Hz. G6 sensor (The sensor closest to the source in the array during monitoring) data from April 4, 2023, shows an average MS soft rock signal in Fig. 4b. Signal duration is 65 ms. The frequency distribution in the time-frequency domain is centered between 234 and 522 Hz. The dominant frequency is 299.333Hz, and the frequency domain curve is smooth with a low peak frequency. The waveform and signal composition are simple. The sensor's sample frequency exceeds two times the monitoring object's primary MS signal's highest frequency, meeting on-site MS monitoring standards.

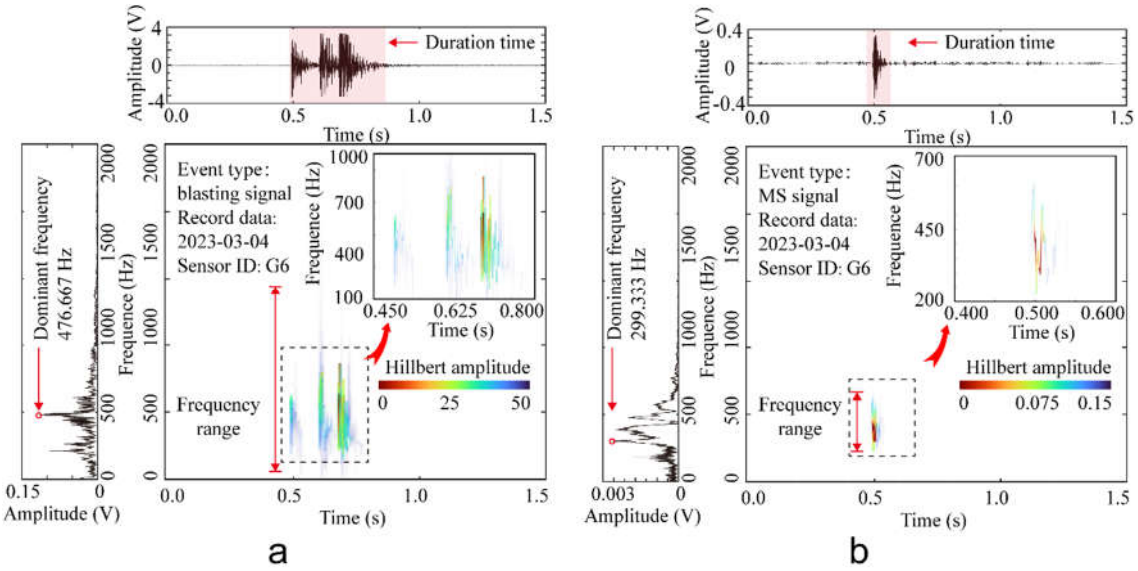


**Figure 3.** Elastic wave signal time domain, frequency domain and spectrum diagram: (a) Typical burst signal. (b) Typical MS signal.

While blasting and MS signal wave shapes are similar, their creation methods differ. a MS signal recognition and classification method combining ensemble empirical mode decomposition (EEMD), singular value decomposition (SVD) and extreme learning machine (ELM) are used to detect microfracture signals automatically in soft rocks (Zhang et al, 2019). This technology gives engineering-useful real-time rock mass fracture data. The study tracked the soft rock tunnel's surrounding rock damage, fracture, and dilatation using real-time online rock micro-fracture data. This MS signal database supports dynamic early warning and analyzes the gradual damage development mechanism of substantial deformation in the soft rock tunnel surrounding rock.

### 2.2 Relationship of the source parameters and Positioning probability density field

Energy transformation is essential to physical changes, and energy drive can cause rock collapse. The energy perspective makes damage evolution analysis evident throughout the rock compression failure. Radiated MS energy comes from elastic waves emitted during rock fracture and sliding due to the transfer of elastic strain energy to inelastic strain energy. Radiated MS energy can show rock microfracture location, intensity, and strain energy storage and release in the focused area. The radiated MS energy [$E$] can be calculated as follows:

$$E = 4\pi\rho v F_c^2 R^2 \int_0^2 \dot{u}_{\text{corr}}^2(t)\mathrm{d}t \tag{1}$$

Where $E$ is the radiated MS energy, $\rho$ is the density of rock mass in the monitoring area, $v$ is the density

of rock mass in the monitoring area, $F_c$ is the root-mean-square radiation pattern factor, $R$ is the focal distance, $t$ is the duration of the MS shape in the time domain, $\dot{u}^2_{corr}(t)$ is the function of the square of the far-field velocity spectrum corrected according to the radiation path.

When more MS events occur during monitoring, the probability density field of each event can be added, resulting in a probability density field of multiple AE events. For all MS events that occur in the measuring time and space range, the probability density at a random location $x$ is calculated as

$$p_A(x) = \sum_{a \in A} f(x, x_{g,a}) = \sum_{a \in A} \frac{1}{(\sqrt{2\pi})} \frac{1}{\sigma^k} e^{-\left\|x - x_{g,a}\right\|^2 / 2\sigma^2}, k \in \{1,2,3\} \quad (2)$$

where, $A$ is a set of all MS events that occurred in the measuring time and space range, $x_{g,a}$ is the estimated location of event $a$, and other parameters are defined same as before. Figure 4 illustrates the whole approach. The required variables/inputs are the arrival times $t_r$, the sensor locations $x_r$, the wave speed $c$ and the standard deviation of the error component $\sigma$. The first three inputs are required for a deterministic source localization, and the last one is needed additionally for a probabilistic source localization.

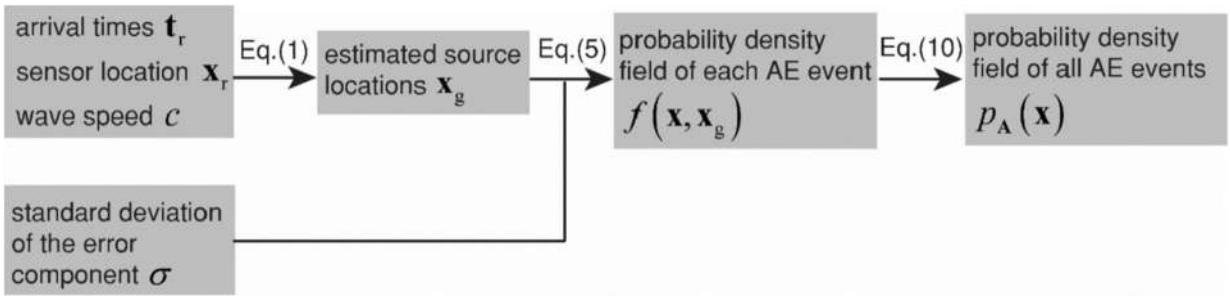


**Figure 4.** Derivation of probability density field of AE events. (Zhang et al., 2022)

## 3 Results

Figure 5a illustrates the temporal-spatial distribution of MS events and deformation at chainage 0+865m–chainage 0+885m section of auxiliary tunnel #4. MS events and deformation of tunnel showed a significant correlation with the advancement of tunnel excavation. The time series is divided into four phases based on three-time points: tunnel step excavation, inverted arch initial support closed loop, and inverted arch pouring. The deformation and MS parameters of all phases are shown in Table 1.

**Table 1.** Deformation parameters and cumulative MS event of all phases

| Parameters | April 1 to 8, 2023 (Phase I) | April 9 to 16, 2023 (Phase II) | April 17 to May 1, 2023 (Phase III) | May 2 to 15, 2023 (Phase IV) |
|---|---|---|---|---|
| Vertical deformation of arch crown / mm | 37.55 | 66.395 | 111.29 | 114.01 |
| horizontal deformation of the arch shoulder / mm | 167.62 | 257.42 | 281.36 | 286.26 |
| horizontal deformation of the arch wasist / mm | 365.99 | 475.10 | 528.44 | 534.69 |
| horizontal deformation of the arch feet / mm | - | 170.07 | 245.71 | 263.40 |
| Cumulative MS event / count | 61.00 | 50.00 | 77.00 | 3.00 |

Phase I corresponds to April 1 to 8, 2023. The deformation data reveals that, following the excavation of the upper partition, the maximum deformation of the tunnel reached 321.7mm in while the average

deformation rate was 40.2 mm/d, located on the arch shoulder. The overall trend of red and blue curve (horizontal deformation of the arch waists and arch feet, respectively) indicates that the surrounding rock has undergone a quick deformation phase, with a few measurement points experiencing abrupt variations. For instance, on April 8, 2023, a peak deformation rate of 70mm/d was detected in a single day. Each day, an average of 7 MS events were recorded, with a maximum of 27 events on the highest day.

Phase II corresponds to April 9 to 16, 2023. The maximum deformation of the tunnel arch waist was 490.9mm, and the average rate was 24.8 mm/d (with a maximum single-day deformation rate of 51.3 mm/d). The average daily MS events were 7, indicating frequent micro- fractures occur. The count of MS events was closely associated with blasting excavation frequency, rock unloading strength, and geological conditions in phase I and II. From April 1 to 16, 2023, the tunnel's internal stress state changed sharply during excavation and unloading in the segment between chainage 0+865 and chainage 0+885, undergoing blasting and mechanical excavation. The excavation would decrease the minimum principal stress in the surrounding rock, causing stress loss and concentrating the maximum principal stress, destroying the surrounding rock of the tunnel and inducing numerous rock micro-fractures.

Phase III corresponds to the time between April 17 to May 1, 2023. The surrounding rock displacement rate reduced dramatically during this stage, and the deformation only reached 40.4 millimeters, averaging 2.7 millimeters per day (maximum 14.7 mm/day). Compared to phase I and II, the frequency of MS activity during phase III has notably decreased, as only an average of 5 MS events were recorded daily. At the same time, the occurrence of MS events decreased progressively over time. It can be inferred from this feature that on the gradual advancement of the excavation working face, the intensity of excavation disturbance lessened, and the associated induced rock fracture activity became relatively weak, resulting in a relatively small count of accompanying MS events.

Phase IV corresponds to the time between May 1 to 15, 2023. This phase has 1.7 mm deformation and 533 mm cumulative deformation. The average daily deformation rate is 0.1 mm. The site construction is mainly supported; the stress of the rock mass tends to be stable, and the whole shows low MS activity. In summary, the convergence deformation growth trend of the surrounding rock is consistent with the time distribution of MS events.

The analysis of the spatial distribution characteristics of AE/MS events offers valuable information about the deformation and damage zone of the surrounding rock resulting from tunnel excavation and unloading (Feng et al., 2023). The spatial distribution of MS events of auxiliary tunnel #4 throughout the monitoring period (April 1 - May 15, 2023) is depicted in Figures 5b and c. The MS events are primarily distributed within a 10m radius of the working face, which indicates that the occurrence of MS events is related to the unloading of tunnel excavation. According to the findings of the tunnel section investigation, it was observed that most MS occurrences tend to concentrate on the east-side wall of the tunnel. Compared to the horizontal convergence deformation data from sections D-E at chainage 0+865m–chainage 0+885m section of auxiliary tunnel #4, the deformation on the west side of the tunnel measures 147.4mm. In comparison, the east side exhibits a displacement of 364.0mm. The deformation failure region of the east side tunnel revealed by MS aggregation agrees with the convergence deformation location (Figure 5c).

Additionally, Figure 5d depicts the measurement of the shortest distance between the center of MS events and the tunnel wall at different phases of tunnel construction. The distance between an MS event and the tunnel wall is considered the shortest distance between an MS source center and the tunnel wall. This approach allows for the analysis of the impact of various MS events on the tunnel wall in space to some extent. In correlation with Figures 5b and c, it can be seen that the excavation of the upper partition leads to the dispersion of MS event throughout the superficial layer of the surrounding rock of the tunnel,

primarily concentrated in the arch crown of tunnel. As the excavation of the upper partition progressed and the initial branch of the invert was sealed, fractures intensified, resulting in notable energy events that propagated from the deep surrounding rock mass and expanded toward the shallow surrounding rock mass.

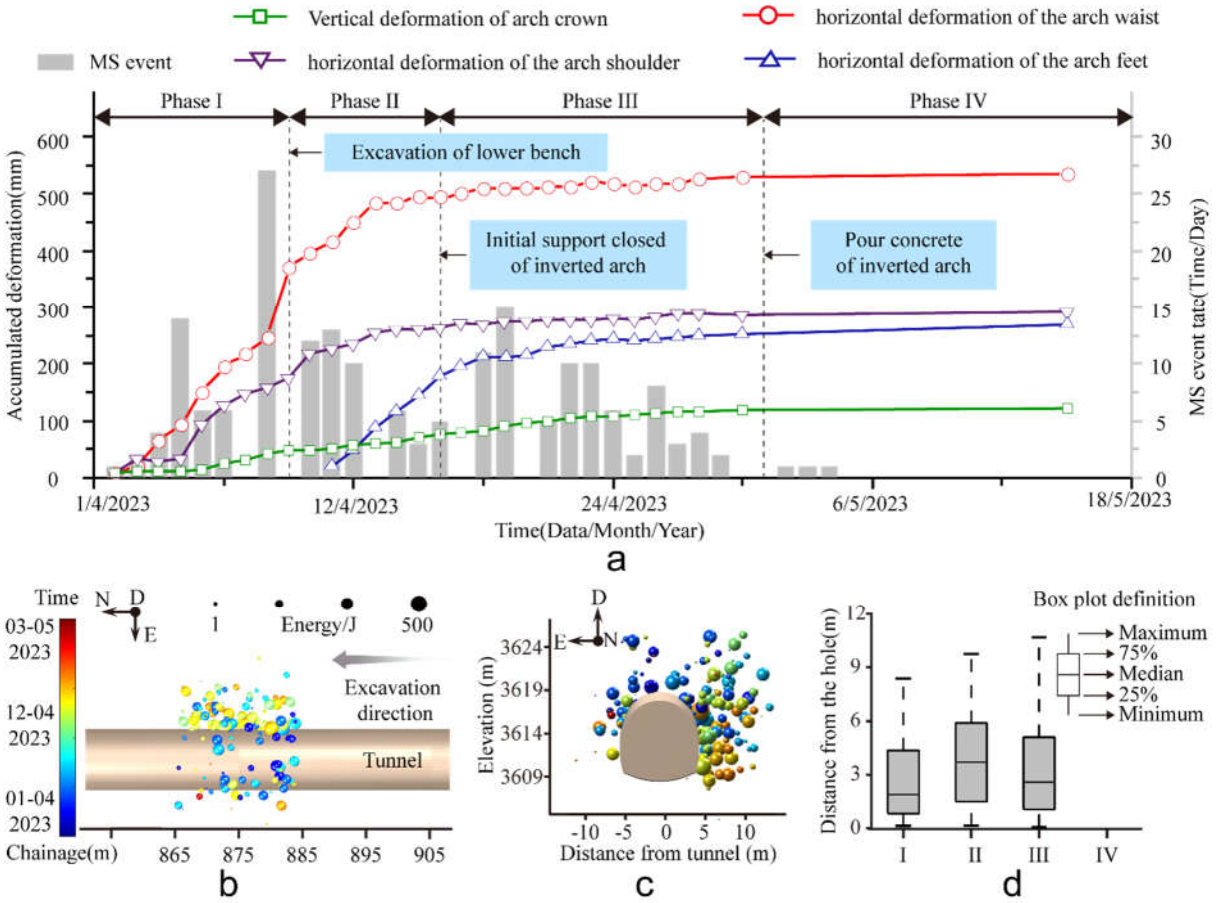


**Figure 5.** Spatial–temporal evolution of the distribution of the MS events: (a) Temporal evolution of MS and deformation of initial support surface. (b) Top view of MS spatial distribution. (c) Front view of MS spatial distribution (the sphere illustrated in the diagram represents the MS event. The different hues represent the temporal occurrence of micro-ruptures, while the magnitude of the sphere is proportional to the radiated MS energy). (d) Statistical rule of MS aggregation.

To further explore the stability of the soft tunnel and forewarn the large deformation caused by stress expansion and structural deformation, author correlate the spatial distribution of radiated MS energy with the damage state of rock mass. The envelope for the radiated MS energy is depicted in Figure 6. The three-dimensional analysis provides spatial distribution and morphological characteristics of the surrounding rock with different damage degrees around the tunnel. Therefore, we can further infer damage areas for potential strong deformation in the soft tunnel rockmass that could be induced by radiated MS energy anomalies. The damage zone of the surrounding rock is asymmetrical in the radial direction of the tunnel, and the damage of the surrounding rock varies in the direction of the tunnel axis with different chainage. This observation is consistent with the results obtained from in-situ deformation monitoring.

The prestressed anchorage support system has achieved a remarkable control effect in soft rock tunnels. This study applies mass spectrometry monitoring to construct three-dimensional models of rock masses with varying degrees of damage. Three high-damage zones are delineated comprehensively, and the depth of deformation zones is generally 4 ~ 12 m. This helps to determine the length of the support (the

length of the anchorage zone passes through the high damage zone) to avoid excessive support strength or insufficient support effectiveness. This approach will aid in managing deformation during the first excavation process and effectively mitigate the resistance encountered by the shotcrete layer's wall support. in addition, based on the visualization of micro-fracture intensity within the surrounding rock's three-dimensional space, the surrounding rockmass damage zone can be specifically targeted using high-strength restrained concrete support to achieve accurate and robust reinforcement for weak surrounding rock.

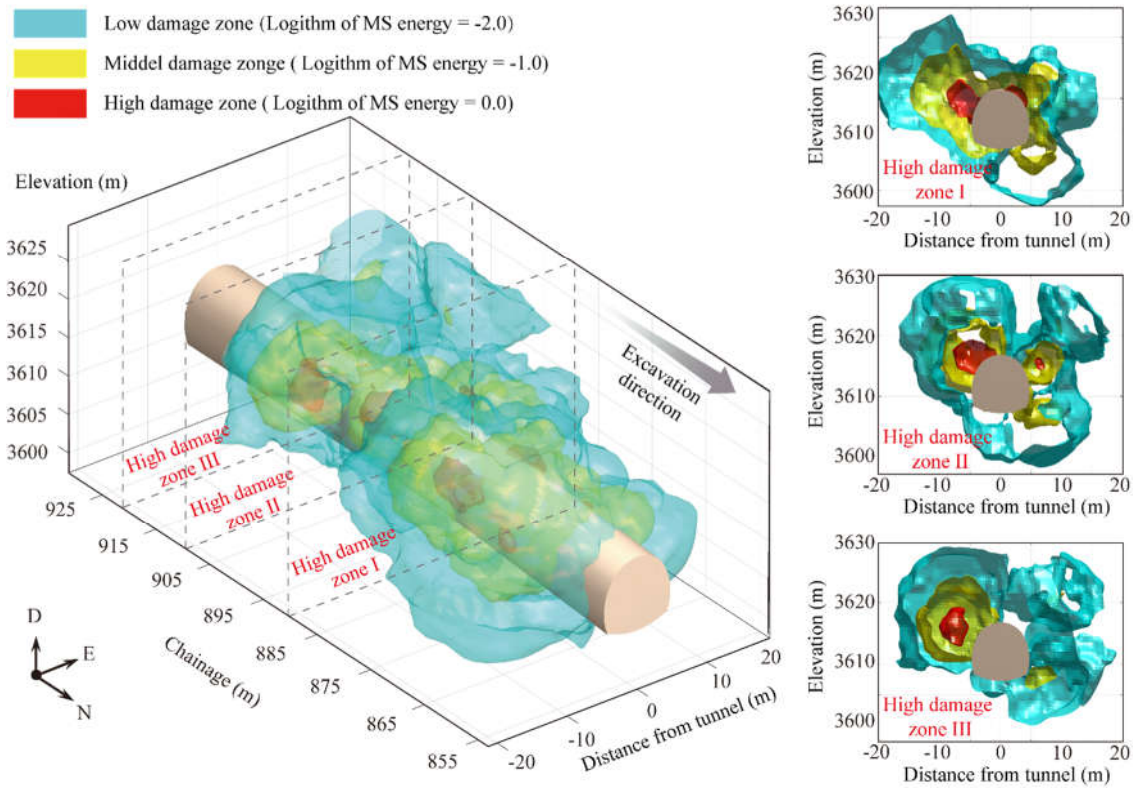


**Figure 6.** The 3D envelope for the radiated MS energy provides spatial distribution and morphological characteristics of the surrounding rock with different damage degrees around the tunnel.

## 4 Conclusion

This paper presents a case study on the plateau soft rock tunnel's progressive deformation and failure mechanism. A comprehensive method integrating the MS monitoring, the numerical simulation, and moment tensor inversion, is applied for a quantitative description of the progressive failure evolution of soft rock tunnel, which involves the fracturing expansion and squeezing deformation of the surrounding rock mass. The conclusions can be drawn.

(1) The aggregation of MS activity, which reflects the progressive damage of the surrounding rock, can better reveal and delineate the deformation and failure area of the soft rock tunnel. During excavation and unloading, MS is distributed throughout the shallow area of the rock surrounding the tunnel, most of it in the top arch region. With excavating the lower partition, the high energy MS event is generated from the deep layer and then propagated shallow.

(2) The research utilizes MS monitoring to create 3D models of rock masses that display different levels of damage. Three regions with significant damage are identified in both the radial and axial directions surrounding the tunnel, with deformation depths typically ranging from 4 to 12 meters.

**Acknowledgements**

We acknowledge the funding support from the National Natural Science Foundation of China (Grant Nos. U23A2060, 42177143 and 42277461) and the Sichuan Science and Technology Program (Grant No. 2023NSFSC0812).

## References

Chen, F., Ma, T.H., Tang, C.A., Du, Y.H., Li, Z.C., Liu, F. Research on the Law of Large-Scale Deformation and Failure of Soft Rock Based on Microseismic Monitoring. *Advances in Civil Engineering*. 2018, 9286758.

Chen, X.Y., Liu, J.L., Burg, J.P., Yan, J.X., Zhou, B.J., Shan, H.S., Bao, X.X., Fan, W.K., Zhang, J., Hou, C.R. Lateral middle-lower crustal flow in response to continental collision: New insights from the metamorphic complexes in the southeastern Tibetan Plateau. Earth-Science Reviews.2023, 247: 104604.

Du, Y.L., Yi, T.H., Li, X.J., Rong, X.L., Dong, L.J., Wang, D.W., Gao, Y., Leng, Z. Advances in Intellectualization of Transportation Infrastructures. *Engineering*. 2023, 24(5): 240-253.

Feng, X.T., Young, R.P., Reyes-Montes, J.M., Aydan, Ö., Ishida, T., Liu, J.P., Liu, H.J. ISRM Suggested Method for In Situ Acoustic Emission Monitoring of the Fracturing Process in Rock Masses. *Rock Mechanics and Rock Engineering*. 2019, 52: 1395-1414.

Feng, X.T., Yang, C.X., Kong, R., Zhao, J., Zhou, Y.Y., Yao, Z.B., Hu, L. Excavation-induced deep hard rock fracturing: Methodology and applications. *Journal of Rock Mechanics and Geotechnical Engineering*. 2022, 14: 1-34.

Hathway, A.W. The Complete ISRM Suggested Methods for Rock Characterization, Testing and Monitoring; 1974–2006. *Environmental & Engineering Geoscience*.2009, 15 (1): 47–48.

He, M.C., Sui, Q.R., Li, M.N. Compensation excavation method control for large deformation disaster of mountain soft rock tunnel. *International Journal of Rock Mechanics and Mining Sciences*. 2022, 32: 951-963.

Kang, Y.S., Geng, Z., Liu, Q.S., Liu, B., Zhu, Y.G. Research progress on support technology and methods for soft rock with large deformation hazards in China. *Rock and Soil Mechanics*. 2022, 43(8): 2035-2059.

Mngadi, S.B., Durrheim, R.J., Manzi, M.S.D., Ogasawara, H., Yabe, Y., Yilmaz, H., Wechsler, N., Van Aswegen, G., Roberts, D., Ward, A.K., Naoi, M. Integration of underground mapping, petrology, and high-resolution microseismicity analysis to characterise weak geotechnical zones in deep South African gold mines. *International Journal of Rock Mechanics and Mining Sciences*. 2019, 114, 79-91.

Wang, L.F., Barbot, S. Three-dimensional kinematics of the India–Eurasia collision. *Communications Earth & Environment*. 2023, 4: 16.

Yu, M.Y., Cheng, F., Liu, J.P., Peng, D.C., Tian, Z.J. Frequency-Domain Full-Waveform Inversion Based on Tunnel Space Seismic Data. *Engineering*. 2022, 18(11): 197-206.

Yu, W., Wang, B., Zi, X., Guo, X.X., Wang, Z.Y. Effect of prestressed anchorage system on mechanical behavior of squeezed soft rock in large-deformation tunnel. *Tunnelling And Underground Space Technology*. 2023, 131: 104782.

Zhang, F.Q., Yang, Y.G., Naaktgeboren, M., Hendriks, M.A.N. Probability density field of acoustic emission events: Damage identification in concrete structures. *Construction and Building Materials* 2022, 327(11): 126984.

Zhang, J.Y., Jiang, R.C., Li, B. An automatic recognition method of microseismic signals based on EEMD-SVD and ELM. *Computers & Geosciences*. 2019, 133:104318.

Zhu, H.H., Yan, J.X., Liang, W.H. Challenges and Development Prospects of Ultra-Long and Ultra-Deep Mountain Tunnel. *Engineering*. 2019, 5(3): 384-392.